npj Computational Materials

www.nature.com/npjcompumats

ARTICLE OPEN

Check for updates

Tunable chemical complexity to control atomic diffusion in alloys

Yuri Osetsky[1]✉, Alexander V. Barashev[2], Laurent K. Béland[3], Zhongwen Yao[3], Keyvan Ferasat[3] and Yanwen Zhang[1,4]

In this paper we report a new fundamental understanding of chemically-biased diffusion in Ni–Fe random alloys that is tuned/controlled by the intrinsic quantifiable chemical complexity. Development of radiation-tolerant alloys has been a long-standing challenge. Here we show how intrinsic chemical complexity can be utilized to guide the atomic diffusion and suppress radiation damage. The influence of chemical complexity is shown by the example of interstitial atom (IA) diffusion that is the most important defect in radiation effects. We use μs-scale molecular dynamics to reveal sluggish diffusion and percolation of IAs in concentrated Ni–Fe alloys. We develop a mean field diffusion model to take into account the effect of migrating defect energy properties on diffusion percolation, which is verified by a new kinetic Monte Carlo approach addressing detailed processes. We demonstrate that the local variations in the ground state energy of IA configurations in alloys, reflecting the chemical difference between alloying components, drives the percolation effects for atomic diffusion. Percolation, chemically-biased and sluggish diffusion are phenomena that are directly related to the chemical complexity intrinsically to multicomponent alloys.

npj Computational Materials (2020)6:38 ; https://doi.org/10.1038/s41524-020-0306-9

INTRODUCTION

Medium- and high-entropy alloys are nearly equiatomic single-phase concentrated solid solution alloys (SP-CSAs)[1–3]. SP-CSAs are a distinct group of concentrated alloys that have tunable chemical complexity[4–6] but lack microstructural inhomogeneities. They have attracted broad attention because of potentially desirable properties, such as high fracture resistance, tensile strength, corrosion resistance, thermal stability, and radiation tolerance[4,5], compared to conventional alloys with one major component. The potential of CSAs as diffusion barriers in the microelectronics industry is also of interest[7,8]. A great amount of experimental information on different properties of CSAs is accumulated, but a complete understanding why different concentrated alloys, sometimes quite close in composition, may exhibit very different diffusion and mechanical behavior, radiation tolerance, and other properties. Theoretical and experimental efforts have been undertaken to understand the mechanisms that control alloy properties. Mixing enthalpy[9,10], defect energetics[11–13], local lattice distortions[13–15], stresses and pressure[16–18], electronic[13,19] and magnetic state disorder[20] were studied. While certain correlations were observed between these properties and alloys performance, clear and predictive models were not developed. Progress was achieved recently in understanding vacancy-based sluggish diffusion in CSAs, which existence was debated for over a decade (see, e.g., pros in refs. [21–23] and cons in refs. [24–26]). The existence and origin of vacancy-based sluggish diffusion[27] were revealed by atomistic simulations. It cannot be explained simply by configurational entropy arguments, as expected earlier (see, e.g., ref. [21]). Consequently, it is not a necessary or exclusive attribute of high-entropy alloys. It exists in alloys with different binding between alloying components and vacancies and occurs when concentration of the element with higher biding approaches the corresponding percolation threshold. In binary Ni–Fe alloys, the maximum sluggish effect for vacancy diffusion mechanism was observed at Fe atomic fraction $C_{Fe} \sim 0.2$[27], which is close to the fcc lattice site percolation threshold. Sluggish diffusion, when present, is also associated with chemically-biased diffusion. These two processes: sluggish and chemically biased diffusion, drive component segregation, creep, defect clustering, nucleation and evolution internal lattice heterogeneities; i.e., practically all aspects of microstructure evolution. As demonstrated in[27], vacancy-based sluggish diffusion is due to a combination of site percolation and composition-dependence of vacancy migration energies. Note that maximum compositional disorder is expected for equiatomic composition, while the maximum chemical complexity depends on the coupling strength of the elements that may involve electron, phonon, magnetic, and mechanical components. Compositional disorder can be described by the elemental concentration whereas the chemical complexity so far has been an ill-defined concept.

In this article, we propose a model that includes the effect of chemical complexity on atomic transport and defect diffusion in CSAs. The measure of chemical complexity in alloys is concretized. μs-scale molecular dynamics (MD) reveal strongly sluggish interstitial atom (IA)-based diffusion in Ni–Fe alloys. It is described as a percolation phenomenon. We develop a mean field model that describes diffusion percolation in alloys on the basis of local energy of migrating defects and analyze the conditions for a variable threshold concentration. We also develop a lattice kinetic Monte Carlo (kMC) model for IA migration with a simple "on-the-fly" definition of the transition states that reproduce the MD results. By cross-verifying theory and kMC results, the local formation energy of migrating defects is revealed to be the parameter controlling the atomic transport. While mixing enthalpy, defect energetics, local lattice distortion, electronic characteristics and magnetic frustration are reported as unique features in CSAs[9–19], this parameter is proposed as the measure of

[1]Materials Science and Technology Division, Oak Ridge National Laboratory, Oak Ridge, TN 37831, USA. [2]Department of Nuclear Engineering and Radiological Sciences, University of Michigan, Ann Arbor, MI 48109, USA. [3]Department of Mechanical and Materials Engineering, Queen's University, Kingston, ON K7L 3N6, Canada. [4]Department of Materials Science and Engineering, University of Tennessee, Knoxville, TN 37996, USA. ✉email: osetskiyyn@ornl.gov

Published in partnership with the Shanghai Institute of Ceramics of the Chinese Academy of Sciences

chemical complexity of the alloys for their observed difference in defect evolution and radiation tolerance[13].

RESULTS

For Ni–Fe alloys the MD-calculated composition dependence of the tracer diffusion coefficient is presented in Fig. 1a, where the diffusion coefficient has a minimum at C_{Fe} ~ 0.50–0.65, with lower values correspond to higher temperature. The phenomenon of sluggish diffusion can be described as a decrease of the total tracer diffusion coefficient, D^*, when adding faster diffusing atoms, Fe, into slower migrating Ni. The effect is strong and, for example, at 500 K the tracer diffusion coefficient decreases by ~20 times with respect to that in pure Ni and by ~500 times relative to pure fcc Fe, i.e., $\min\{D^*_{NiFe}\} \approx 0.05 D^*_{Ni} \approx 0.002 D^*_{Fe}$. A more detailed treatment of the MD results was performed to investigate the composition dependence of the partial diffusion coefficients (D^*_{Ni} and D^*_{Fe}), their activation energies (E^m_{Ni} and E^m_{Fe}) and chemical composition of migrating <100> interstitial dumb-bells (d-b). In other words, we investigate the chemical configuration of migrating <100> interstitial dumb-bells and their surrounding environment, as well as their corresponding their activation energies, in order to reveal the composition dependence of the partial diffusion coefficients. This treatment indicates that the diffusion percolation occurred near the $\min\{D^*_{NiFe}\}$ composition, p_c, as illustrated in Fig. 1b, c. Thus, in this Ni–Fe system at 500 K, $p_c \approx 0.7$ ($C_{Fe} \approx 0.7$). Figure 1b shows that the composition dependences of the partial diffusion coefficients, $D^*_{Ni}(C_{Fe})$ and $D^*_{Fe}(C_{Fe})$, intersect just after the p_c, when Fe atom diffusion becomes dominant in the atomic transport. Figure 1c demonstrates that this transition is directly related to the change in chemical composition of the migrating <100> d-b: before p_c the dumb-bells contain only Ni atoms, whereas at $C_{Fe} > p_c$ the dumb-bells contain increasingly more Fe, resulting in accelerated transport of Fe-atoms. Note that the equality of the partial diffusivities and dumb-bells chemical composition occurs at C_{Fe} ~0.7, which is well above the equiatomic composition, where one expects the maximum chemical disorder. This is a clear demonstration of the chemically-biased diffusion when the migrating interstitial defects provide preferential transport of Ni atoms even in Fe-rich alloys. Some evidence of the slow and chemically-biased diffusion observed in DFT and classical MD calculations of IA diffusion in equiatomic alloys have been reported recently[28–30], however, a complete picture of the sluggish diffusion phenomenon, percolation and their composition dependence is reported here for the first time.

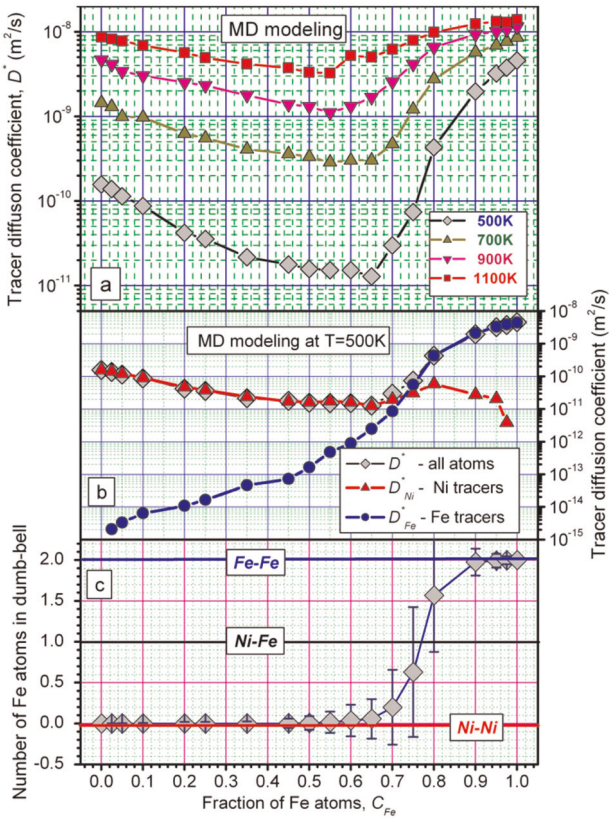

Fig. 1 MD modeling of interstitial atom diffusion in Ni–Fe random alloys. a Composition dependence of the tracer diffusion coefficients for different temperatures. Evidence of percolation phenomena in MD modeling of interstitial atom diffusion in Ni–Fe alloys. **b** Composition dependence of the total, D^*, and partial Ni, D^*_{Ni}, and Fe, D^*_{Fe}, tracer diffusion coefficients at 500 K. **c** Composition dependence of Fe content in the migrating <100> dumb-bells modeled by MD at 500 K. Error bars indicate the standard deviation obtained in the treatment of up to 10^6 individual configurations after each detected jump. Ni–Ni dumb-bell corresponds to "0", Ni–Fe to "1" and Fe–Fe configuration corresponds to "2" as indicated on the plot.

Existence of a non-monotonic composition dependence of the diffusion coefficient and the percolation threshold at C_{Fe} ~0.65–0.70 is not consistent with any of the models and mechanisms considered so far. The percolation theory is developed for different cases and the percolation threshold concentrations are estimated for different lattice structures (see, e.g., ref. [31]). For example, the vacancy diffusion studied in[27] corresponds to the site percolation model quite accurately: simulations suggest that Fe are the faster than Ni, and the percolation is observed at C_{Fe} ~ 0.2, consistent with the fcc lattice site percolation threshold $p_{site} = 0.18$[31]. The interstitial migration via <100> d-b mechanism in the fcc lattice was studied theoretically in ref. [32] and the percolation threshold concentration, $p_{d\text{-}b} = 0.72$, was estimated. In the case of IA migration studied here, diffusion in pure Fe is faster than in pure Ni, and one expects a similar value for p_c. However, the most currently accurate MD modeling of interstitial atom diffusion described above resulted in a quite different percolation threshold concentration $p_c \approx 0.65$–0.70 which is clearly associated with the minimum of the composition dependent diffusion coefficient D^*. The significant difference between $p_c \approx 0.65$–0.70 and $p_{d\text{-}b} = 0.72$ calls for attention to chemically-biased atomic motions.

Theoretical model

To elucidate possible contributions to such a discrepancy, we developed a mean-field theoretical model that takes into account some of the basic physical properties of defects in chemically complex solutions. The aim is to find out how the migrating defect properties contribute to upper level processes, such as percolation and sluggish diffusion. These phenomena are associated here with alloys' chemical complexity. The model considers binary alloys with the atomic fractions C_i (i = A, B): $C_A + C_B = 1$, where the migrating defect can be in two, A and B, ground states (equivalent to Ni–Ni and Fe–Fe dumb-bells) and in the transition states between them. Therefore, it operates with three parameters which are two migration energies, E^m_{AA} and E^m_{BB}, and the energy difference between the ground states, $\Delta E^f = E^f_B - E^f_A$ (see Fig. 2a). The diffusion coefficient is obtained by the thermodynamic averaging of the defect jump frequencies

$$D = D_0\left(p_A\langle B\rangle^m_{Aj} + p_B\langle B\rangle^m_{Bj}\right), \quad (1)$$

where D_0 is the pre-exponential factor of the diffusion coefficient, p_i is the probability that site i is occupied by a defect, and $\langle B\rangle^m_{ij}$ is the Boltzmann factor for defect jump from ground state i, averaged over different atomic configurations of j atoms

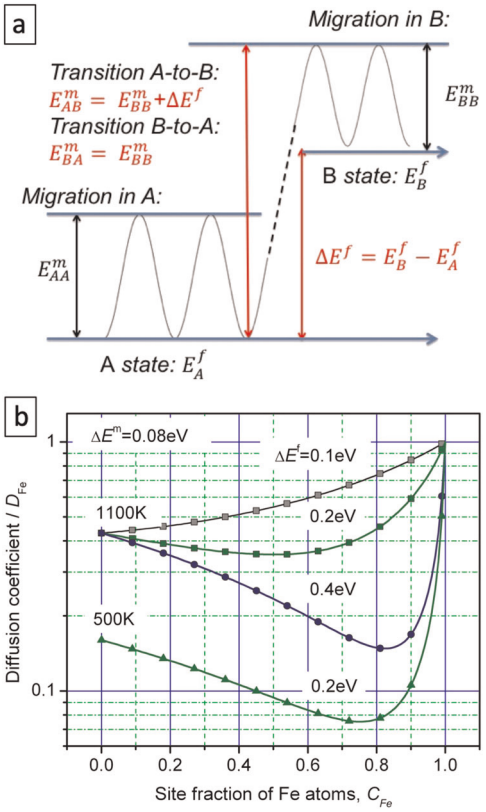

Fig. 2 Theoretical model parameters and results. a Qualitative presentation of energy profile along a migrating defect trajectory. Two states A and B are characterized with formation, E^f_A and E^f_B, and migration, E^m_{AA} and E^m_{BB}, energies. Transition A-to-B requires activation energy $E^m_{AB} = E^m_{BB} + \Delta E^f$ whereas B-to-A requires only $E^m_{BA} = E^m_{BB}$ as shown. **b** Composition dependence of the diffusion coefficient predicted by the theoretical model for different parameters. $\Delta E^m = 0.08$ eV is the difference of interstitial atom migration energy in pure Ni ($E^m_{Ni} = 0.35$ eV) and Fe ($E^m_{Fe} = 0.27$ eV), obtained for the interatomic potentials used here. ΔE^{mf} is the difference in formation energies between the distinctive states A and B considered in the model.

surrounding ground state. The occupation probability of states by a migrating defect is

$$p_i = \frac{C_i B^f_i}{C_A B^f_A + C_B B^f_B}, \tag{2}$$

where $B^f_i = \exp(-\beta E^f_i)$, E^f_i is the formation energy of state i, $\beta^{-1} = k_B T$, T the absolute temperature and k_B the Boltzmann constant. In the mean-field approximation we replace averaging over different atomic configurations surrounding ground state by the value corresponding to a single state with neighboring atoms for the alloy-averaged atomic concentrations:

$$\langle B \rangle^m_{ij} = C_A B^m_{iA} + C_B E^m_{iB}, \tag{3}$$

where $B^m_{ij} = \exp(-\beta E^m_{ij})$, E^m_{ij} is the activation energy of jump from i to j states.

The diffusion scenario is illustrated in Fig. 2a, where the subsystem B is chosen to have higher defect formation energy (which makes it similar to Fe in Ni–Fe alloy). As indicated in the figure, in this case, $E^m_{BA} = E^m_{BB}$ and $E^m_{AB} = E^f_B - E^f_A + E^m_{BB}$, and only two independent parameters define the ratio $\langle D \rangle / D_B$ (where $D_B = D_0 f_{BB}$), in addition to temperature:

$$\Delta E^f = E^f_B - E^f_A, \tag{4}$$

$$\Delta E^m = E^m_{AA} - E^m_{BB}. \tag{5}$$

Now we can combine Eqs. (1)–(3) to obtain the main equation

$$\frac{\langle D \rangle}{D_B} = \frac{1}{B_m} \frac{C_A^2 + (1 - C_A^2) B^{SD}}{C_A + (1 - C_A) B^f}, \tag{6}$$

where $B^m = \exp(-\beta \Delta E^m)$, $B^f = \exp(-\beta \Delta E^f)$ and $B^{SD} = \exp(-\beta \Delta E^{SD})$, $\Delta E^{SD} = E^{SD}_B - E^{SD}_A$ being the difference of the self-diffusion energies: $E^{SD}_i = E^f_i + E^m_i$.

By differentiating Eq. (6) over C_A, one finds that at certain conditions there is a minimum in the concentration dependence of the diffusion coefficient. So, is $B^f \ll B^m$, and the position of the minimum is located at

$$C^{min}_A \approx \sqrt{B^{SD}}, \tag{7}$$

Note that the percolation effects (ignored here) must shift the minimum of diffusion coefficient to lower A-atom concentrations for A-rich alloys and to higher B-atom concentrations for B-rich alloys. This is because the long-range diffusion needs transition jumps between A and B subsystems when approaching the corresponding percolation thresholds.

It follows from Eq. (7) that, for the minimum to be located at B-atom concentration higher than p_c and lower than 1-p_c, ΔE^{SD} must not be too high; otherwise the minimum will coincide with the percolation threshold 1-p_c for faster Ni atoms. Also, taking into account the percolation effects on long-range diffusion, ΔE^f must be larger than ΔE^m; otherwise the migration energy difference will prevail, and the minimum will coincide with the percolation threshold p_c of faster B atoms, as in the conventional approaches for site percolation[27,31]. The diffusion properties of such a system were estimated using Eq. (3) for conditions close to those of the MD modeling. We considered two temperatures 1100 K and 500 K, $\Delta E^m = 0.08$ eV (the interatomic potentials used in MD modeling[33] provides $E^m{}_{Ni} = 0.35$ eV and $E^m{}_{Fe} = 0.27$ eV) and different values of ΔE^f. Note that the static estimations of defect energies show large spectra of the ground states (see kMC section below), and different energy jumps will be realized depending on the temperatures. The probability of more energetic jumps increases with increasing temperature, but the probability of low energy jumps is always higher. In the model presented here, we use: $\Delta E^f = (0.1 \div 0.4)$ eV that is within the range considered below in kMC modeling. The results are presented in Fig. 2b. The conclusions of the theoretical analysis are as follows:

i. The minimum in the concentration dependence of D^*_{NiFe} in Fe–Ni alloys is explained by competition of two processes: faster migration of Ni in Ni-rich alloys due to higher stability of Ni–Ni d-b and faster migration of Fe in Fe-rich alloys due to lower migration energy, $E^m_{Fe} < E^m_{Ni}$.
ii. The minimum of D^*_{NiFe} is located at Fe concentrations between p_c and 1-p_c due to an enhanced probability of energetic transitions between Fe and Ni subsystems at these concentrations.
iii. To observe such a minimum, ΔE^f must be larger than ΔE^m; otherwise it will coincide with the percolation threshold p_c for faster Fe atoms, as in the conventional models[25,26], and
iv. $\Delta E^{SD} = \Delta E^f + \Delta E^m$ must be not too high; otherwise it will coincide with the percolation threshold 1-p_c for faster Ni atoms.

Lattice kMC model

In the above theoretical model we considered only two transition states which are not exactly correlated with the dumb-bell migration mechanism where the three states AA, AB, and BB

a

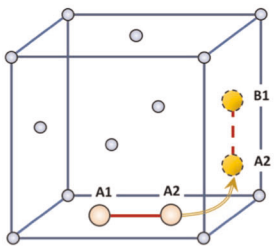

b

E^a	A1	A2	B1
E^m_{Ni}	Ni	Ni	Ni
E^m_{Ni} - (<E_{NiNi}> - <E_{NiFe}>)	Ni	Ni	Fe
E^m_{Fe}	Ni	Fe	Ni
E^m_{Fe}	Fe	Fe	Fe
E^m_{Fe} + (<E_{NiFe}> - <E_{FeFe}>)	Fe	Fe	Ni
E^m_{Ni} + (<E_{NiNi}> - <E_{NiFe}>)	Fe	Ni	Ni
E^m_{Ni}	Fe	Ni	Fe
E^m_{Fe} - (<E_{NiFe}> - <E_{FeFe}>)	Ni	Fe	Fe

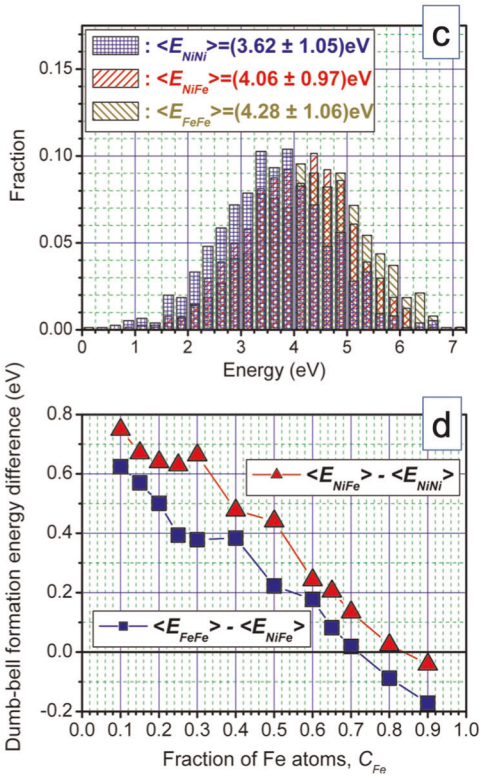

Fig. 3 Transition states for <100> dumb-bell migration in Ni–Fe alloys. a Schematic presentation of A1-A2->A2-B1 dumb-bell jump. Eight jumps, that is combinations of A1, A2 and B1, are possible in two-component alloys. **b** Table of transition state energies, E^a, calculated for different jumps of interstitial atom in in the form of <100> dumb-bell in Ni–Fe alloys. E^m_{Ni} and E^m_{Fe} are interstitial atom migration energies in pure Ni and Fe. <E_{NiNi}>, <E_{NiFe}>, and <E_{FeFe}> are mean energies for Ni–Ni, Ni–Fe and Fe–Fe dumb-bells calculated from the corresponding energy distributions. Parameters used in kMC modeling for "on-the-fly" estimation transition state energies for interstitial atom migration in Ni–Fe alloys. **c** Distribution of formation energies of different <100> dumb-bells estimated in the equiatomic NiFe alloy. Energies for each configuration were estimated using static modeling of >700 different random distributions of the same number of Ni and Fe atoms. Energies are presents relatively to the global minimum energy over all the distributions and dumb-bells. Mean energies and their standard deviations are shown for all three dumb-bell types in the inset. **d** Composition dependence of differences of mean formation energies of different dumb-bells: <E_{NiFe}>−<E_{NiNi}> (red triangles) and <E_{FeFe}>−<E_{NiFe}> (blue squares). Positive value means increasing transition state energy for the corresponding dumb-bell jump.

may occur. A more accurate description can be obtained by the kMC that takes into account these details. The transition state energy in this kMC model is defined by (1) which, Ni or Fe, atom jumps with corresponding migration energy barrier E^m_{Ni} or E^m_{Fe}, respectively; and (2) the configuration energy gain for the process occurred, ΔE, that can be equal to 0, $\pm E_1$ or $\pm E_2$.

The ground state configuration of IAs in fcc lattice is <100> dumbbell and it can consist of different alloying atoms. The possible <100> dumb-bell jumps in a binary alloy are depicted in Fig. 3a. For each current dumbbell composition A1-A2 after either A1 or A2 atom jumps exist three possible compositions such as A2-A2, A1-A1, and A1-A2. Considering three possible initial configurations in the binary alloys considered here: Ni–Ni, Ni–Fe, and Fe–Fe, one can estimate eight possible transition states. In the first approximation, each transition state energy can be estimate as $E^a = E^m + \Delta E$, where E^m is the barrier for the corresponding atom displacement and ΔE is the energy change due to the change in the interstitial configuration: This is nothing more than the Bell-Evans-Polanyi principle[34] applied to the specific case considered here. An estimation of activation energies of the possible eight transition states is shown in Fig. 3b. As E^m we used barriers estimated in pure Ni and Fe as presented above. Contribution from interstitial atom formation energy difference depends on the particular configuration change. Only two energies are necessary to consider the possible cases, namely $<\Delta E_1> = <E_{NiFe}> - <E_{FeFe}>$ and $<\Delta E_2> = <E_{NiFe}> - <E_{NiFe}>$. Here E_{NiFe}, E_{FeFe}, and E_{NiNi} are formation energies of Ni–Fe, Fe–Fe, and Ni–Ni dumbbells correspondingly. While E^m depends only on the migrating atoms i.e., Ni or Fe, the above dumbbell formation energies depend on the alloy's composition. We calculated these energies for different compositions: $C_{Fe} = 0.1 - 0.9$ using static modeling. For each composition we model Ni–Ni, Ni–Fe, and Fe–Fe dumb-bells in crystals with exactly the same number of Ni and Fe atoms distributed randomly. Over 700 different atomic distributions were tested for the each dumb-bell type. The energy difference between each configuration and the global minimum among all energies was calculated for the each dumb-bell type. An example of distributions of these energies calculated for the equiatomic alloys is presented in Fig. 3c. The inset indicates the mean values for the each dumb-bell type and one can see that Ni-Ni dumb-bells have a minimum energy, 3.62 eV, followed by 4.06 eV for Ni–Fe dumb-bell and, finally, Fe–Fe dumb-bell has the maximum mean energy equal to 4.28 eV. These values can be interpreted in the following way. For example, initial Fe–Fe dumb-bell jumped into configuration with Fe–Ni composition. The energy balance of this process in average is: $<\Delta E> = <\Delta E_1> = <E_{NiFe}> - <E_{FeFe}> = -0.22$ eV which means that when Fe-atom from the Fe–Fe dumb-bell jumps towards Ni-atom and creates Fe-Ni dumbbell the total crystal energy decrease. The transition state energy for such processes is $E^a = E^m + <\Delta E> = 0.05$ eV. The composition dependence of $<\Delta E_1>$ and $<\Delta E_2>$ is presented in Fig. 3d. In the case when $<\Delta E_1> = <\Delta E_2>$ the theoretical and the

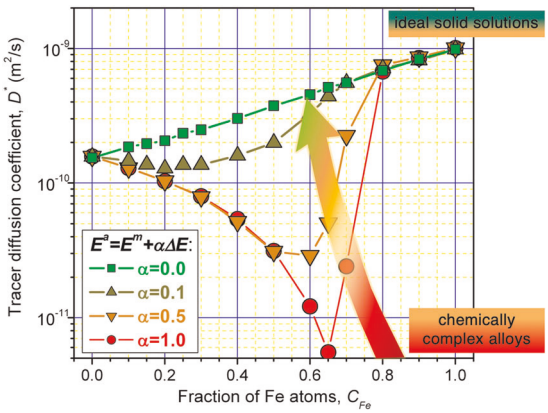

Fig. 4 kMC modeling for investigating the effect of local dumb-bell formation energy, Δ*E*, to the compositional dependence of tracer diffusion coefficient. Block-arrow indicates direction of decreasing chemical complexity of the alloying components when decreasing of energy difference of dumb-bell in different states transforms chemically complex alloy into ideal solid solution.

kMC models are equivalent. For the interatomic potentials used here to describe Ni–Fe system[33] the difference between these energies is ~(0.1–0.2) eV and weakly depends on composition (see Fig. 3c, d). In general, dumb-bells have affinity to Ni-atoms, which makes the above theoretical approach qualitatively correct.

To investigate the effect of chemical complexity on atomic transport, we performed kMC modeling with the variable contribution from the difference in local energy to the transition state energy of a migrating dumb-bell: $E^a = E^m + \alpha\Delta E$. The parameter α here controls the contribution from the defect local energy, which is composition dependent (see Fig. 3). The resulting composition dependence of the tracer diffusion coefficient is presented in Fig. 4 for α (i.e., the quantifiable parameter of chemical complexity) = 1, 0.5, 0.1, and 0. $\alpha = 1$ corresponds to alloy with a high level of chemical complexity, resulting in very strong effects of percolation, sluggish and chemically-biased diffusion. This is the case of a high stability of Ni–Ni dumb-bells over other configurations. In this case the Fe diffusion percolation occurs at the site percolation threshold C_{Fe} between 0.70 and 0.80 (hence C_{Ni} ~ 0.20–0.30) when a continuous dumb-bell migration, via Ni–Ni-to-Ni–Ni jumps, is no longer possible. The sudden increase of Fe atoms appearance in the dumb-bells presented in Fig. 1c is a clear demonstration of Fe-atoms diffusion percolation. The shape of the composition dependence of D^* obtained by kMC (red circles in Fig. 4) reproduces fairly well the MD results (gray diamonds in Fig. 1a). Lower α, i.e., lower alloy's chemical complexity, results in decreasing percolation and sluggish diffusion effects and shifting the percolation threshold concentration towards lower Fe contents. At $\alpha = 0$, the tracer diffusion coefficient becomes a linear function of the alloy composition, realizing an ideal alloy that is predicted by conventional theory with only compositional effects but little or none chemical effects.

For simplicity, we considered initially random solid solutions, which is a common assumption in the high entropy alloys community. This case is related to high temperature states of SP-CSAs, whereas at low temperatures a certain level of local chemical order (LCO) forms in many materials. Inclusion of LCO in direct molecular dynamics modeling would require significant increase of the modeling system to include necessary spectrum of particular LCO configurations. This demands huge computational resources, well beyond even the unprecedented μs-scale MD modeling used in the present work. Extended studies of the defects properties in LCO configurations can produce necessary data from lattice Monte Carlo models, similar to that used here, and the role of LCO can be studied at this level. We predict that the LCO will minimize the local free energy and, therefore, local defect formation energy, acting as an additional contribution into the defect effective migration energy E^a considered above, increasing its value and, thus, the entire effect of chemical complexity. An indirect evidence of this can be found in the recent study of the LCO effects to dislocation glide in SP-CSAs[35], where it was demonstrated that the LCO heightens the ruggedness of the energy landscape and raises the activation barriers governing dislocation activity. There is also a report of kinetic Activation Relaxation Technique simulations of vacancy and SIA diffusion in ordered and disordered Ni-based alloys that provide evidence to this effect[36]. We expect qualitatively similar effects on the defects' long-range diffusion.

The percolation and chemically-biased diffusion of IAs described here, coupled to the concentration-dependence of vacancy migration in SP-CSAs[27], most likely have an important effect on radiation-induced point-defect recombination, as well as interaction of point-defects with extended defects—such as dislocation-type structures. Such effects can be captured in concentrated alloys over experimental timescales by techniques such as the kinetic Activation Relaxation Technique[37].

DISCUSSION

The theoretical and kinetic Monte Carlo analysis of molecular dynamics data on interstitial atom diffusion in Ni–Fe alloys presented here lead to the following important conclusions:

1. Percolation effects on sluggish and chemically-biased diffusion and composition dependence of the tracer diffusion coefficient in real alloys are determined by the variation of local energies, surrounding environment and chemistry of the migrating defects.
2. In particular, the minimum in the concentration dependence of D^*_{NiFe} in Fe–Ni alloys is explained by competition of preferential migration of Ni in Ni-rich alloys due to higher stability of interstitial dumbbell and faster migration of Fe in Fe-rich alloys due to lower migration energy.
3. The distribution of local defect energies is the measure of the quantifiable alloy chemical complexity for atomic diffusion;

Beyond various measures of complexity in such concentrated alloys discussed in the literature, such as mixing enthalpy[9,10], defects energy[11,12] and local atomic distortions[13,14] we added a new metric: the formation and migration energy of local defect configurations. A novel, direct, link was established between defect energies distributions and transport properties of concentrated alloys. Chemical complexity of the alloy and the underlying mechanisms for the composition dependent percolation observed and described here i.e., sluggish and chemically-biased diffusion, can be estimated using the theoretical and Monte Carlo models proposed here with a limited set of energy properties of migrating defects, which can be obtained through classical or ab initio atomistic modeling.

METHODS

Atomistic modeling of diffusion in concentrated alloys

Atomic scale methods and mean field theory of diffusion used in this research to study interstitial atom diffusion in Ni–Fe alloys. The empirical potentials for the fcc Ni–Fe alloys developed in ref. [33], which are consistent with the DFT-defined properties of point defects, were used in MD modeling of thermally activated IA diffusion and static modeling of interstitial formation and migration energies.

Molecular dynamics

Molecular dynamics (MD) is an ideal tool for studying dynamic properties of atomic systems evolving at finite temperature with internal and external

driving forces (see e.g.,[38,39]. for general information), however, currently, only classical MD methods based on Newtonian equations, in conjunction with empirical interatomic potentials (IAPs) are able to model point defect diffusion over long enough time to provide sufficient statistics of elementary migration events–defect jumps. Microsecond-scale MD simulations have been applied here to study IA diffusion in fcc-type Ni–Fe alloys. Concentrated alloys impose new diffusion mechanisms that (a) decelerate interstitial atom diffusion, (b) introduce new strong correlations in IA jumps and (c) demand much greater statistics of interstitial atom jumps for results to converge. As we have found here the sluggish diffusion effect in Ni–Fe system is much stronger for IA migration than for vacancy migration. The origin of this is a higher stability of Ni containing <100> dumb-bell configurations in fcc Ni–Fe alloys (see Fig. 3c above). This leads to a strongly correlated diffusion when the interstitial atom in dumb-bell configuration keeps trying to jump to Ni–Ni sites and therefore long defect trajectories must be model to reproduce the representative statistics of defect configurations. Here we present results on modeling unprecedently long defect diffusion trajectories of up to ~10^6 jumps of the IA over up to ~5 μs physical time. We have modeled thermally activated migration of interstitial atoms in fcc pure Ni and Fe and 17 alloys with Fe concentrations in atomic fraction: $C_{Fe} = 0.025$, 0.05, 0.1, 0.2, 0.25, 0.35, 0.45, 0.5, 0.55, 0.6, 0.65, 0.7, 0.75, 0.8, 0.9, 0.95, and 0.975 over a temperature range 500–1100 K. A large number of alloys was necessary to, first, investigate relatively dilute alloys and, second, accurately define the sluggish diffusion composition range. The general approach to treat MD data is described elsewhere[38]. An important part of defect diffusion treatment is understanding correlations in defect jumps. These correlations depend on the local environment including composition fluctuations and local chemical order (LCO). A migrating defect should visit a large number of different lattice sites to account for all possible correlations and ensure that its diffusion coefficient saturates for long range diffusion. Two techniques for defect trajectory analysis were applied here: TJD-trajectory jumps decomposition, when the whole defect trajectory is decomposed into segments of the same number of jumps, N_j, and TTD–trajectory time decomposition, when the trajectory is decomposed into segments of equal time, t_s (see ref. [38] for details). The overal defect diffusion coefficient, D^d, is defined as the mean over the all trajectory segments in the corresponding statistical treatment. Analysis of D^d behavior versus segment length allows to estimate the scale of correlations in the diffusion process. As can be seen from the Fig. 5, for interstitial atom migrating in the equiatomic alloy at 500 K the diffusion coefficient estimated in TTD and TJD treatments saturate in the same value, $D^d = (6.2 \pm 0.3) \times 10^{-11}$ m^2/s, for segments longer than $t_s \approx 1.5$ ns that, in average, include more than $N_j \approx 300$ jumps. The trajectory decomposition parameters, t_s and N_j, define the scale of correlations in interstitial atom diffusion. Modeling conditions in this particular case, i.e., >10^6 interstitial atom jumps and ~4.8 μs physical time, mean that the interstitial atom diffusion trajectory consists of >3×10^3 segments that, in average, include necessary fluctutaions and correlations, and provide a high accuracy in estimating the overall diffusion properties. In the current research we operated mainly with tracer diffusion coefficients, D^*, D^*_{Ni}, and D^*_{Fe}, that are defined by treating the corresponding atomic square displacements (ASD) as function of simulated time (see ref. [40] for details). An example of ASDs and their treatment is presented in Fig. 6, where one can see that all ASDs can be accurately approximated by linear functions vs time (Fig. 6a), and this provides an accurate Arrhenius law parameterization for the temperature dependent tracer diffusion coefficients (Fig. 6b).

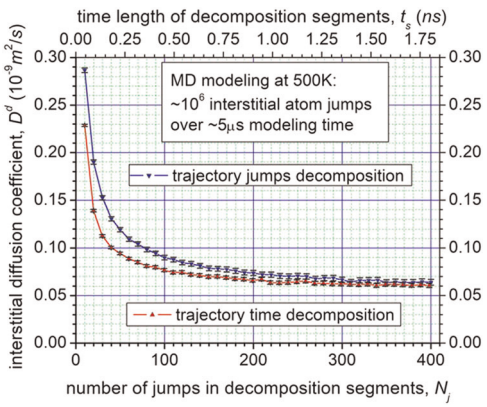

Fig. 5 Analysis of MD data. Interstitial diffusion coefficients in equiatomic NiFe alloy estimated at 500 K using different trajectory decomposition techniques: defect diffusion coefficients saturate to the same value for segments of $N_j > 300$ jumps in TJD and $t_s > 1.5$ ns in TTD.

Theoretical model

In an alloy with infinite ratio of the partial diffusion coefficients, the tracer diffusion coefficient reaches its minimum at concentration of faster species equal to the site percolation threshold, p_c (=0.72 for the interstitial dumbbell diffusion on the fcc crystal lattice[32]). In a real, 'gray', hence more percolating, system, the minimum of the diffusion coefficient (or change of its slope) must be shifted to lower concentrations.

In contrast, in Fe–Ni, where Ni atoms are faster in Ni-rich alloys due to higher stability of interstitial defect and Fe atoms are faster in Fe-rich alloys due to lower migration energy, the minimum of the diffusion coefficient is found at Fe concentrations higher than p_c and lower than 1- p_c, which are the percolation thresholds for faster Fe and Ni atoms, respectively. Hence, the origin of the effect must be different from that of the classical percolation. For this reason and for simplicity, below we ignore percolation effects.

Lattice kMC model

KMC modeling interstitial atom migration in concentrated alloy is rather complicated for the activation energy for elemental interstitial atom (<100> dumb-bell here) jumps is relatively low, ~0.1–0.3 eV, while the difference in energy of <100> dumb-bell in different positions in a concentrated alloy may be well above an eV as demonstrated for example in refs. [12,27] for the equiatomic NiFe alloy. The general description of kMC

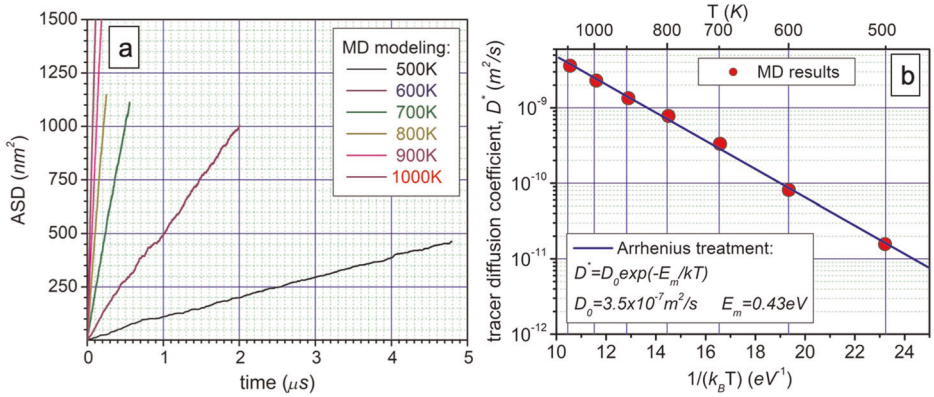

Fig. 6 MD modeling results for tracer diffusivity by interstitial atom mechanism in the equiatomic NiFe alloy. a–temporal evolution of atomic square displacements (ASD) at different temperatures; **b**–tracer diffusion coefficients obtained from Fig. 6a and their Arrhenius law parameterization.

approach can be found elsewhere[41]. Here we developed a version of lattice kMC model where transition states for particular configurations are estimated during modeling on the basis of statistically averaged local energies of different interstitial configurations.

In practice, during the "on-the-fly" kMC modeling of interstitial atom diffusion in NiFe alloys, the following steps were performed:

(1) Generate a cubic fcc crystal with dimensions $10a \times 10a \times 10a$ with a random distribution of Ni and Fe atoms of a particular composition, with a <100> dumb-bell in the center;
(2) Identify the four nearest neighbors for each dumb-bell atom A1 and A2 (see Fig. 3a);
(3) Calculate the possible transition states and E^a for A1 and A2 atoms jumps according to Fig. 3a, b;
(4) Execute a kMC step according to the reaction chosen for the simulated temperature among the estimated transition state energies;
(5) Go to step (2).

For all the reactions modeled by kMC we used a constant attempt frequency (2.5 THz) that was estimated by fitting kMC results on tracer diffusivity of <100> dumb-bell in pure Ni at 500 K to the corresponding results obtained by MD.

DATA AVAILABILITY

The authors declare that the data supporting the findings of this study are available within the paper. Requests for materials, including data that support the plots within this paper and other findings of this study, are available from the corresponding author (osetskiyyn@ornl.gov) upon reasonable request.

CODES AVAILABILITY

The computer codes used are available upon request from authors: MD from Yuri Osetsky osetskiyyn@ornl.gov and kMC from Keyvan Ferasat 17kf7@queensu.ca.

Received: 12 August 2019; Accepted: 10 March 2020;
Published online: 21 April 2020

REFERENCES

1. Yeh, J.-W. Alloy design strategies and future trends in high-entropy alloys. *J. Mater.* **65**, 1759–1771 (2013).
2. Tsai, M.-H. & Yeh, J.-W. High-entropy alloys: a critical review. *Mater. Res. Lett.* **2**, 107–123 (2014).
3. Lim, X. Mixed-up metals make for stronger, tougher starchier alloys. *Nature* **533**, 306–307 (2016).
4. Gludovatz, B. et al. A fracture resistance high-entropy alloy for cryogenic applications. *Science* **345**, 1153–1158 (2014).
5. Granberg, F. et al. Mechanism of radiation damage reduction in equiatomic multicomponent single phase alloys. *Phys. Rev. Lett.* **116**, 135504 (2016).
6. Zhang, Y. et al. Microstructures and properties of high-entropy alloys. *Prog. Mater. Sci.* **61**, 1–93 (2014).
7. Chang, S. Y., Chen, M. K. & Chen, D. S. Multiprincipal-element AlCrTaTiZr-nitride nanocomposite film of extremely high thermal stability as diffusion barrier for Cu metallization. *J. Electrochem. Soc.* **156**, G37–G42 (2009).
8. Tsai, M.-H. et al. Thermal stability and performance of NbSiTaTiZr high-entropy alloy barrier for copper metallization. *J. Electrochem. Soc.* **158**, H1161–H1165 (2011).
9. Troparevsky, M. C., Morris, J. R., Kent, P. R. C., Lupini, A. R. & Stocks, M. Criteria for predicting the formation of single-phase high-entropy alloys. *Phys. Rev. X* **5**, 011041 (2015).
10. Troparevsky, M. C. et al. Beyond atomic sizes and hume-rothery rules: understanding and predicting high-entropy alloys. *J. Mater.* **67**, 2350–2363 (2015).
11. Yeh, J.-W. Physical metallurgy of high-entropy alloys. *J. Mater.* **67**, 2254–2261 (2015).
12. Zhao, S., Stocks, G. M. & Zhang, Y. Defect energetics of concentrated solid-solution alloys from ab initio calculations: $Ni_{0.5}Co_{0.5}$, $Ni_{0.5}Fe_{0.5}$, $Ni_{0.8}Fe_{0.2}$ and $Ni_{0.8}Cr_{0.2}$. *Phys. Chem. Chem. Phys.* **18**, 24043–2456 (2016).
13. Zhang, Y., Egami, T. & Weber William, J. Dissipation of radiation energy in concentrated alloys: unique defect properties and microstructural evolution. *MRS Bull.* **44**, 798 (2019).
14. Ye, Y. F., Wang, Q., Lu, J., Liu, C. T. & Yang, Y. High-entropy alloys: challenges and prospects. *Mater. Today* **19**, 349–362 (2016).
15. Wang, Z., Qiu, W., Yang, Y. & Liu, C. T. Atomic-size and lattice-distortion effects in newly developed high-entropy alloys with multiple principal elements. *Intermetallics* **64**, 63–69 (2015).
16. Zhang, Y. et al. Atomic-level heterogeneity and defect dynamics in concentrated solid-solution alloys. *Curr. Opin. Solid State Mater. Sci.* **21**, 221–237 (2017).
17. Tong, Y. et al. Severe local lattice distortion in Zr/Hf-containing refractory multi-principal element alloys. *Acta Mater.* **183**, 172–181 (2019).
18. Oh, H. S. et al. Engineering atomic-level complexity in high-entropy and complex concentrated alloys. *Nat. Commun.* **10**, 2090 (2019).
19. Zhang, Y. et al. Effects *3d* electron configurations on helium bubble formation and void swelling in concentrated solid-solution alloys. *Acta Mater.* **181**, 519–529 (2019).
20. Mu, S., Yin, J., Samolyuk, G. D., Wimmer, S. & Eisenbach, M. et al. Hidden Mn magnetic-moment disorder and its influence on the physical properties of medium-entropy NiCoMn solid solution alloys. *Phys. Rev. Mater.* **3**, 014411 (2019).
21. Tsai, K.-Y., Tsai, M.-H. & Yeh, J.-W. Sluggish diffusion in Co–Cr–Fe–Mn–Ni high-entropy alloys. *Acta Mater.* **61**, 4887–4897 (2013).
22. Rohrberg, D. et al. Host atom diffusion in ternary Fe-Cr-Al alloys. *Metall. Mater. Trans. A* **45**, 269–279 (2014).
23. Dabrowa, J. et al. Interdiffusion in the FCC-structured Al-Co-Cr-Fe-Ni high entropy alloys: experimental studies and numerical simulations. *J. Alloy. Compd.* **674**, 455–462 (2016).
24. Miracle, D. B. & Senkov, O. N. A critical review of high entropy alloys and related concepts. *Acta Mater.* **122**, 448–511 (2017).
25. Paul, Aloke Comments on "Sluggish diffusion in Co–Cr–Fe–Mn–Ni high-entropy alloys" by K.Y. Tsai, M.H. Tsai and J.W. Yeh. *Acta Mater.* **61**, 4887–4897 (2013).
26. Kucza, W. et al. Studies of "sluggish diffusion" effect in Co-Cr-Fe-Mn-Ni, Co-Cr-Fe-Ni and Co-Fe- n-Ni high entropy alloys; determination of tracer diffusivities by combinatorial approach. *J. Alloy. Compd.* **731**, 920–928 (2018).
27. Osetsky, Y. N., Béland, L. K., Barashev, A. V. & Zhang, Y. On the existence and origin of sluggish diffusion in chemically disordered concentrated alloys. *Curr. Opin. Solid State Mater. Sci.* **22**, 65–74 (2018).
28. Barnard, L. & Morgan, D. *Ab initio* molecular dynamics simulation of interstitial diffusion in Ni-Cr alloys and implications for radiation induced segregation. *J. Nucl. Mater.* **449**, 225–233 (2014).
29. Osetsky, Y. N., Béland, L. K. & Stoller, R. E. Specific features of defect and mass transport in concentrated fcc alloys. *Acta Mater.* **115**, 364–371 (2016).
30. Zhao, S., Osetsky, Y. N. & Zhang, Y. Preferential diffusion in concentrated solid solution alloys: NiFe, NiCo and NiCoCr. *Acta Mater.* **128**, 391–399 (2017).
31. Xu, X., Wang, J.-P. & Deng, Y. Simultaneous analysis of three-dimensional percolation models. *Front. Phys.* **9**, 113–119 (2014).
32. Bocquet, J. L. Percolation diffusion of a dumbbell interstitial defect on a fcc lattice: calculation of a percolation threshold with use of a series method. *Phys. Rev. B* **50**, 16386 (1994).
33. Bonny, G., Terentyev, D., Pasianot, R. C., Ponce, S. & Bakaev, A. Interatomic potential to study plasticity in stainless steels: the FeNiCr model alloy. *Model. Simul. Mat. Sci. Eng.* **19**, 085008 (2011).
34. Evans, M. G. & Polanyi, M. Further considerations on the thermodynamics of chemical equilibria and reaction rates. *J. Chem. Soc. Faraday Trans.* **32**, 1333–1360 (1936).
35. Li, Q.-J., Sheng, H. & Ma, E. Strengthening in multi-principal element alloys with local-chemical-order roughened dislocation pathways. *Nat. Commun.* **10**, 3563 (2019).
36. Mahmoud, Sami & Mousseau, Normand Long-time point defect diffusion in ordered nickel-based binary alloys: How small kinetic differences can lead to completely long-time structural evolution. *Materialia* **4**, 575–584 (2018).
37. Béland, Laurent., Karim, GermanD., Samolyuk. & Roger, E. Stoller. Differences in the accumulation of ion-beam damage in Ni and NiFe explained by atomistic simulations. *J. Alloy. Compd.* **662**, 415–420 (2016).
38. Rapaport, C. M. *The Art of Molecular Dynamics Simulation* (Cambridge University Press, 2004).
39. Leach, A. *Molecular Modelling: Principles and Applications* (Pearson, 2001).
40. Osetsky, Y. N. Atomistic study of diffusional mass transport in metals. *Defect Diff. Forum* **188–190**, 71–92 (2001).
41. Leetmaa, M. & Skorodumova, N. V. KMCLib: a general framework for lattice kinetic Monte Carlo (KMC) simulations. *Comput. Phys. Commun.* **185**, 2340–2349 (2014).

ACKNOWLEDGEMENTS

This work was supported as part of the Energy Dissipation to Defect Evolution (EDDE), an Energy Frontier Research Center funded by the U.S. Department of Energy, Office

of Science, Basic Energy Sciences under contract number DE-AC05-00OR22725. A part of this work was funded by the Natural Science and Engineering Research Council. L.K.B. and K.F. thank Compute Canada for generous allocation of computer resources. This manuscript has been authored by UT–Battelle, LLC under Contract No. DE–AC05–00OR22725 with the U.S. Department of Energy. The United States Government retains and the publisher, by accepting the article for publication, acknowledges that the United States Government retains a non-exclusive, paid-up, irrevocable, world-wide license to publish or reproduce the published form of this manuscript, or allow others to do so, for United States Government purposes. The Department of Energy will provide public access to these results of federally sponsored research in accordance with the DOE Public Access Plan.

AUTHOR CONTRIBUTIONS

Y.O. conceived the idea, performed MD modeling and drafted the manuscript, L.K.B., Z.Y., and K.F. performed kMC modeling, A.V.B. and Y.O. performed theoretical analysis. Y.Z. envisioned connection to experimental results and implications. All the authors contributed to the discussion of the project and manuscript preparation. Y.Z. and Y.O. have finalized the manuscript.

COMPETING INTERESTS

The authors declare no competing interests.

ADDITIONAL INFORMATION

Correspondence and requests for materials should be addressed to Y.O.

Reprints and permission information is available at http://www.nature.com/reprints

Publisher's note Springer Nature remains neutral with regard to jurisdictional claims in published maps and institutional affiliations.